

High-corrosion-resistant Al₂O₃ passivation-film formation by selective oxidation on austenitic stainless steel containing Al

Masafumi Kitano, Hidekazu Ishii, Yasuyuki Shirai, and Tadahiro Ohmi

Citation: *J. Vac. Sci. Technol. A* **29**, 021002 (2011); doi: 10.1116/1.3543709

View online: <http://dx.doi.org/10.1116/1.3543709>

View Table of Contents: <http://avspublications.org/resource/1/JVTAD6/v29/i2>

Published by the AVS: Science & Technology of Materials, Interfaces, and Processing

Related Articles

In situ fabrication of blue ceramic coatings on wrought Al Alloy 2024 by plasma electrolytic oxidation
J. Vac. Sci. Technol. A **30**, 021302 (2012)

Influence of substrate temperature and bias voltage on properties of chromium nitride thin films deposited by cylindrical cathodic arc deposition
J. Vac. Sci. Technol. A **29**, 051515 (2011)

Ultrathin TiSiN overcoat protection layer for magnetic media
J. Vac. Sci. Technol. A **29**, 051502 (2011)

Low-energy ion bombardment to tailor the interfacial and mechanical properties of polycrystalline 3C-silicon carbide
J. Vac. Sci. Technol. A **28**, 1259 (2010)

Microstructure and tribological performance of nanocomposite Ti–Si–C–N coatings deposited using hexamethyldisilazane precursor
J. Vac. Sci. Technol. A **28**, 1126 (2010)

Additional information on *J. Vac. Sci. Technol. A*

Journal Homepage: <http://avspublications.org/jvsta>

Journal Information: http://avspublications.org/jvsta/about/about_the_journal

Top downloads: http://avspublications.org/jvsta/top_20_most_downloaded

Information for Authors: http://avspublications.org/jvsta/authors/information_for_contributors

ADVERTISEMENT



K-Alpha XPS System
Maximize productivity.

[Learn more >](#)

Thermo
SCIENTIFIC

High-corrosion-resistant Al₂O₃ passivation-film formation by selective oxidation on austenitic stainless steel containing Al

Masafumi Kitano,^{a)} Hidekazu Ishii, Yasuyuki Shirai, and Tadahiro Ohmi

New Industry Creation Hatchery Center, Tohoku University, Aramaki Aza-Aoba 6-6-10, Aoba-ku, Sendai, Japan

(Received 26 April 2010; accepted 20 December 2010; published 14 January 2011)

We have developed Al₂O₃ passivation film having very high anticorrosion resistance on the surface of austenitic stainless steel containing 3 wt % aluminum. Al₂O₃ passivation film is formed by selective oxidation of aluminum in the austenitic stainless steel in the Ar and H₂ ambient including a small amount of H₂O at predetermined temperatures. Al₂O₃ film is obtained at temperatures higher than 750 °C in the Ar and H₂ ambient, where the partial pressure ratio of H₂ and H₂O is set higher than 2×10^3 . Al₂O₃ films have been confirmed to exhibit very high anticorrosion resistance for various halogen gases and various plasma ambients (Cl₂, H₂, and O₂) with ion-bombardment energies less than 100 eV at temperatures less than 150 °C. In the case of fluorine-gas plasma, the Al₂O₃ film surface has been converted to AlF₃ with a depth of 15 nm, where AlF₃ film is thermodynamically stable, as well as Al₂O₃, resulting in an excellent passivation film exhibiting very high anticorrosion capability. Moreover, the Al₂O₃ film surface has been confirmed to exhibit no catalytic activity for various specialty gases at temperatures less than 150 °C. © 2011 American Vacuum Society. [DOI: 10.1116/1.3543709]

I. INTRODUCTION

Silicon technology is now getting into the era of GHz frequency operation and very high-performance system large-scale integration (LSI). The high-*k* gate dielectric, low-*k* dielectric interconnect, metal gate, and metal substrate silicon-on-insulator (SOI) structure is a unique solution to the GHz frequency operation Si system LSI. Present processes around the transistor fabrications are carried out at high temperatures (about 1000 °C) using molecules such as oxygen (O₂) and water vapor (H₂O) having low reactivity. In this method, it is impossible to introduce the metal-substrate SOI structure. This is because the problems of cracking and warpage arise from the difference in the coefficient of thermal expansion. It is reported that low-temperature transistor-fabrication processes are established by very-well-regulated high-density plasma completely free from contamination and damages,¹⁻⁷ resulting in total low-temperature processes (less than 600 °C), such as low-temperature radical oxidation and radical nitridation of the Si surface, low-temperature growth of various films, and various film etchings. So, metal substrate SOI LSI manufacturing will become feasible by introducing these total low-temperature processes based on newly developed plasma equipment free from various contaminants and damage. In order to establish high-quality total plasma-process equipment free from various fluctuations, chemically stable material surfaces are essentially required for the gas-supply system, the process chambers, the gas pumps, and exhaust-gas duct system, i.e.,

- (1) High corrosion resistance for various gases, radicals, and ions.

- (2) A chemically stable surface having no catalytic activity and free from various specialty gases' decomposition.

Metal contamination from the gas-supply system or the process chamber to the substrate degrades LSI performance and manufacturing yield. Also, the corrosion of pumping system or deposition of by-product on the exhaust inner duct causes a fluctuation of pumping performance. Under these conditions, reproducible processes are difficult to obtain.

In the case of aluminum alloy, it has been confirmed that attempting the anodic oxidation of Al₂O₃ films by using non-aqueous solutions demonstrates very high corrosion resistance in various gas and plasma environments.^{8,9} On the other hand, there is very limited reporting of stainless-steel surface passivation to satisfy previously described conditions. It has been reported that Cr₂O₃ passivation film on ferritic stainless-steel exhibits very strong anticorrosion resistance for halogen gas ambients such as HCl, Cl₂, and HBr.^{10,11} However, in the case of a plasma environment having strong reactivity, Cr₂O₃ film is corroded or etched away by active ions and radicals. For example, after Cr₂O₃ is oxidized by O radicals and O₃ ambients, it converts to CrO₃, where CrO₃ has a high vapor pressure and it disappears from the stainless-steel surface. Thus, the transition metal has various oxidation numbers. And, passivation film formed with transition-metal compounds has various phases. The property becomes completely different by the oxidation number. So, it is not appropriate to use a transition-metal compound for a passivation film. It is reported that stainless-steel covered by Al₂O₃ film can be made by the method of selective oxidation.¹² Al is not a transition metal, so Al₂O₃ passivation film is very excellent if it is obtained on a stainless-steel surface.

^{a)}kitano@fff.niche.tohoku.ac.jp

TABLE I. Chemical composition of stainless steel used in this study.

Al containing austenitic stainless steel	Composition (wt %)								
	Cr	Ni	Mo	Mn	Al	C	S	P	Fe
	17.7	21.0	0.01	<0.01	3.0	<0.01	<0.01	<0.01	Remain

In this paper, we will describe the forming condition of Al₂O₃ passivation films on the surface of austenitic stainless steel containing 3 wt % aluminum. Moreover, we have investigated the property of Al₂O₃ passivation films, such as anticorrosion resistance for plasma environments and catalytic behavior for various specialty gases.

II. EXPERIMENT

The specimens used in this study were high-purity 25Ni-18Cr-3Al steel. The composition of new austenitic stainless steel is shown in Table I. Figure 1 shows the schematic diagram of the experimental setup used to evaluate the condition of Al₂O₃ film formation. Oxidation was performed in a H₂/H₂O environment diluted with Ar. Our gas-distribution system was capable of introducing H₂ and O₂ gases diluted with Ar to a predetermined concentration into an oxidation furnace. The total gas-flow rate was 1 l/min. The moisture is synthesized in the moisture-generation reactor made up of Ni by the reaction of H₂ and O₂ gases. The oxidation furnace is composed of infrared heating by halogen lamp and it can be controlled uniformly below 1000 °C. The film thickness and the chemical composition of the films were examined by depth-profile x-ray photoelectron spectroscopy (XPS) using a Shimadzu ESCA-1000S with Mg-K α radiation.

Welding cannot be avoided in the fabrication of the gas supply and exhaust tubing system. The mechanism of welding is to create molten metal and to connect them together. Meanwhile, the passivation film is removed during the welding process. So, the welding process needs to reform the passivation film on the welded bead while carrying out the welding process. We explored the conditions for forming an Al₂O₃ film formed condition on the welded bead while employing automatic welding process with a high-speed one path welding method developed in our laboratory.¹³

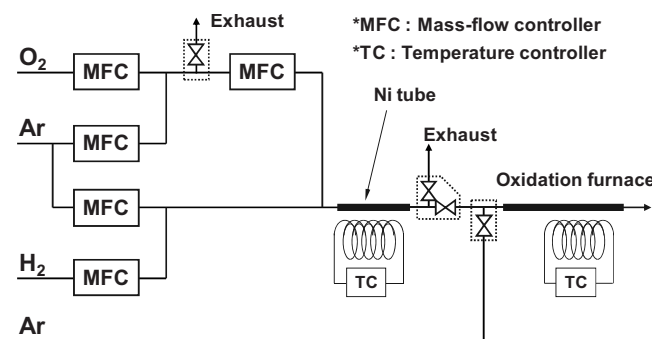


FIG. 1. Schematic diagram of the experimental setup to evaluate the Al₂O₃ film-formation condition.

The schematic diagram of the welding experiment is shown in Fig. 2. This system was made up of a backshield gas line, an arc-shield gas line, and welder head. The backshield gas plays the role of keeping inner pressure of the welding tube and maintaining the tube diameter of the molten part in the appropriate size. The internal pressure of the welding tube was measured and controlled by using a differential-pressure gauge set in the outlet end of the welding tube. And, the arc-shield gas plays the role of keeping the arc discharge stable and preventing the outside of the tube from being burned out. The reason for the H₂ gas addition into the Ar gas was to reduce the heat input for the arc discharge, as well as to reduce the formation of chromium carbide taking place at the grain boundaries of the heat-affected zone. An arc autowelder (Model 207A) made by Arc-Machine, Inc. was used for this experiment. Ten percent H₂/Ar gas with a flow rate of 12 l/min was used for the arc-shield gas.

The single-path butt-weld technique was employed with the various backshield gas ambient. The welding-sample material size used in this research had an outer diameter of 6.35 mm and wall thickness of 1 mm. The type of gas and the concentration of backshield gas used in this experiment are only the Ar, or 5% H₂ in the Ar, or trace amounts of oxygen in the Ar. The rotating speed of the welded electrode was fixed at 30 rotations/min and the single path with bead width was 1 mm. Optimum welding current and welding duration were examined so as to make the welded bead smooth.

The plasma-irradiation test of the Al₂O₃ film was performed using a parallel-plate plasma-excitation apparatus. In this system, the ion-bombardment energy at the substrate was controlled by adjusting the applied radio-frequency (rf) power with the frequency of 13.56 MHz. We have experimented in the range of ion-bombardment energy below 130 eV. This experiment was carried out at a gas pressure of 2.7

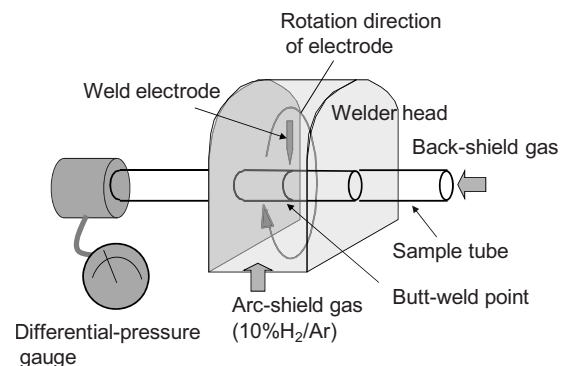


FIG. 2. Schematic diagram of the tube welding.

TABLE II. Standard enthalpy of formation and standard Gibbs free energy of formation of various oxides and fluorides.

Oxide	ΔH_f^0	ΔG_f^0	Fluoride	ΔH_f^0	ΔG_f^0
PbO	-85		NiF ₂	-651	-604
CuO	-157	-130	FeF ₂	-661	-619
NiO	-244	-216	FeF ₃	-1000	
MnO	-385	-363	CrF ₂	-774	-732
MoO ₂	-520	-465	CrF ₃	-1154	-1088
SnO ₂	-581	-520	MgF ₂	-1123	-1070
Fe ₂ O ₃	-824	-752	AlF ₃	-1502	-1425
SiO ₂	-911	-857			
TiO ₂	-913	-890			
Fe ₃ O ₄	-1118	-1015			
Cr ₂ O ₃	-1140	-1058			
Al ₂ O ₃	-1675	-1582			
Ta ₂ O ₅	-2046	-1911			
Ti ₃ O ₅	-2445	-2318			

 ΔH_f^0 : Standard enthalpy of formation ΔG_f^0 : Standard Gibbs free energy of formation unit: kJ/mol

Pa. The gas for various plasmas with the flow rate of 5 ml/min supported by 45 ml/min Ar was introduced from the gas-delivery line (the total flow rate into the test chamber was 50 ml/min). The change in film thickness and the chemical composition of the films were examined by XPS measurement. The surface observation of the passivation film was investigated by scanning-electron microscopy (SEM) observation using a JEOL JSM-6401F. We evaluated by comparing the conventional austenitic SUS316L-Electro Polish (EP) surface and 20 nm of Cr₂O₃ passivation film surface on ferritic stainless steel, these are generally used in semiconductor manufacturing equipment.⁹

For catalytic-effect evaluation, the sample tube was 6.35 mm in outer diameter, 1 mm in thickness, and 1 m in length. The sample tube had a volume of 15 cm³ and an inner surface area of 137 cm². We evaluated by comparison with the conventional austenitic SUS316L-EP surface and the Ni surface. These sample tubes were purged by Ar gas for 1 h at 500 °C to remove the adsorbed moisture from the inner surface. We evaluated the catalytic effect of the surfaces for SiH₄, B₂H₆, PH₃, AsH₃, and ClF₃ decomposition. These gases diluted with Ar at 100 ppm and 5 cm³/min flowed individually through the tube. Then the temperature was raised to 550 °C (at 1 °C/min) to evaluate above gas-thermal decomposition. Gas concentration was monitored by Fourier-transfer infrared spectroscopy (FT-IR).

III. RESULTS AND DISCUSSION

A. Al₂O₃ passivated film formation

Table II shows the standard enthalpy of formation of various materials. The standard enthalpy of formation of Al₂O₃ has large absolute value compared with other materials. It shows that Al₂O₃ passivation film is thermodynamically very stable. Furthermore, Al is the typical element and the phase does not change after the film formation. So, we focused on Al₂O₃ passivation film.

The oxidation of metal is generally given by the following equation:



The standard Gibbs free energy of formation (ΔG^0) of this reaction is as follows:

$$\Delta G^0 = -RT \ln K = -RT \ln \{(a_{M_xO_y}^{2/y}) / (a_M^{2x/y} P_{O_2})\}, \quad (2)$$

where R is the gas constant of an ideal gas (8.31 J/K mol), T is a temperature, K is an equilibrium constant, a is an activity, and P is a dissociation pressure. ΔG^0 is related to the equilibrium oxygen-dissociation pressure and the temperature when the activity value of pure metal and metal oxide are one:

$$\begin{aligned} \Delta G^0 &= -RT \ln K = -RT \ln \{(a_{M_xO_y}^{2/y}) / (a_M^{2x/y} P_{O_2})\} = \\ &= -RT \ln(1/P_{O_2}) = RT \ln(P_{O_2}). \end{aligned} \quad (3)$$

$RT \ln(P_{O_2})$ is called the oxygen potential. The oxygen potential is related to the dissociation pressure ratio between hydrogen and moisture (P_{H_2}/P_{H_2O}). This is shown as follows:



$$\Delta G^0 = -RT \ln(P_{H_2O}^2 / P_{H_2}^2 \times P_{O_2}), \quad (5)$$

$$RT \ln P_{O_2} = \Delta G^0 - RT \ln(P_{H_2}^2 / P_{H_2O}^2). \quad (6)$$

From these equations, the oxidation-reduction reaction is determined by the controlling P_{H_2}/P_{H_2O} ratio and the temperature. For example, the oxidation-reduction reaction of Al-Al₂O₃ in the H₂/H₂O atmosphere is given by the following equation. Fe, Ni, and Cr are also shown by the similar equation:



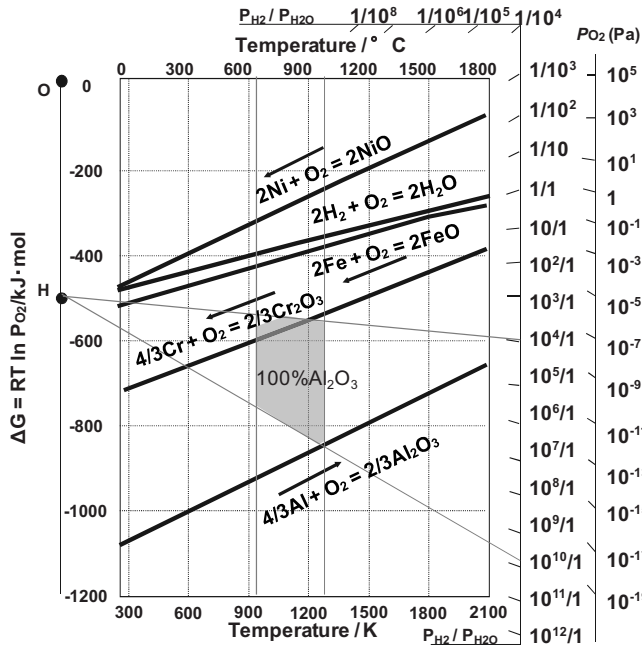
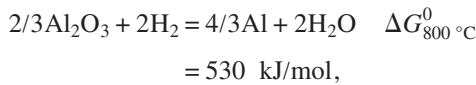


FIG. 3. Some relevant oxidation-reduction equilibrium curves (Ellingham diagram).



$$\Delta G_{1073 \text{ K}}^0 = 530 \text{ 000} = -8.31 \times 1073 \times 2.303 \times \log \frac{P_{\text{H}_2\text{O}}^2}{P_{\text{H}_2}^2},$$

$$\therefore P_{\text{H}_2}/P_{\text{H}_2\text{O}} = 8 \times 10^{12}. \quad (7)$$

In the case of $P_{\text{H}_2}/P_{\text{H}_2\text{O}} = 1 \times 10^5$ atmosphere with 800 °C, the equilibrium of reaction (7) moves to the direction that consumes the moisture. In other words, the oxidation of Al is generated. On the contrary, $P_{\text{H}_2}/P_{\text{H}_2\text{O}}$ of Eq. (8) is calculated to 4×10^4 at 800 °C:



In the case of $P_{\text{H}_2}/P_{\text{H}_2\text{O}} = 1 \times 10^5$ with 800 °C, equilibrium of Eq. (8) moves to the direction that consumes the hydrogen. In short, the reduction in Cr₂O₃ occurred. In the case of

Fe and Ni, there occurs a similar reaction as with Cr. In this way, the stable state of each element is decided by the H₂/H₂O gas-mixing ratio and the temperature. Figure 3 shows some relevant oxidation-reduction equilibrium curves based on Ellingham's work in 1944, which was developed by Richardson and Jeffes.^{14,15} From this figure, it is easily possible to judge the equilibrium state of the various oxides in the predetermined $P_{\text{H}_2}/P_{\text{H}_2\text{O}}$ ratio and applied temperature. In our experiments, in the area of $P_{\text{H}_2}/P_{\text{H}_2\text{O}}$ ratio and temperature shown in Fig. 3, 100% Al₂O₃ film free from Fe, Cr, Ni, and Mo elements composing stainless-steel was completely formed. It is described herein. Surprisingly, it was almost exactly consistent with the data of Ellingham's diagram, experimentally acquired more than 60 years ago. The importance of Ellingham's work was felt even more keenly.

Figures 4(a) and 4(b) show the XPS depth profile before and after the oxidized stainless-steel surface with $P_{\text{H}_2}/P_{\text{H}_2\text{O}} = 1 \times 10^4$ at 900 °C for 30 min. The horizontal axis shows film thickness and the vertical axis shows atomic concentration. Before oxidation, the XPS profile indicates a normal stainless-steel surface such as native chromium-rich-oxide surface. However, after oxidation, only Al and O are detected up to 60 nm, showing that Al₂O₃ passivation film is formed by these oxidation procedures. From the binding energy of the XPS spectrum (not shown), the chemical states of Fe, Cr, and Ni under 60 nm from the surface are confirmed as metallic, rather than oxidized ions indicating that the oxide is etched off by a H radical or reduced by Al in some regions of the surface. Al₂O₃ passivation film thickness without Cr, Fe, and Ni is defined as 100% Al₂O₃ passivation-film thickness. We investigated the formation condition of a 100% Al₂O₃ passivation film. Figure 5 shows the relationship between 100% Al₂O₃ film thickness and $P_{\text{H}_2}/P_{\text{H}_2\text{O}}$ at 800 °C for 1-h treatment. It is shown that the 100% Al₂O₃ film is formed at $P_{\text{H}_2}/P_{\text{H}_2\text{O}}$ above 2×10^3 . In the case of the ratio under 2×10^3 , a Cr₂O₃ passivation film is also formed within the Al₂O₃ film. Figure 6 shows the relationship between 100% Al₂O₃ passivation-film thickness and treatment temperature for 30 min with $P_{\text{H}_2}/P_{\text{H}_2\text{O}} = 1 \times 10^5$. It is shown that the 100% Al₂O₃ passivation film is formed above 750 °C. Below 750 °C, Cr₂O₃ film is also formed with Al₂O₃ film.

In our study, in the environment with $P_{\text{H}_2}/P_{\text{H}_2\text{O}} \cong 2 \times 10^3$ with the temperature over 750 °C (lower than

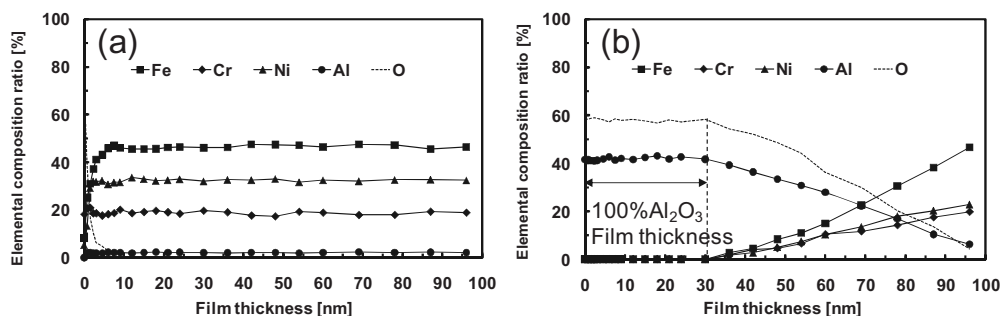


FIG. 4. (a) XPS depth profile of stainless-steel surface before oxidation of surface. (b) XPS depth profile of after-oxidization stainless-steel surface in the ambient of $P_{\text{H}_2}/P_{\text{H}_2\text{O}} = 1 \times 10^4$ at 900 °C for 30 min.

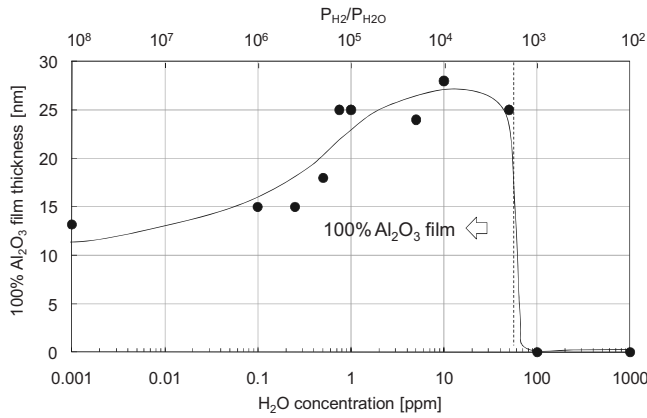


FIG. 5. Relationship between 100% Al₂O₃ film thickness and P_{H_2}/P_{H_2O} ratio at 800 °C for 1 h treatment.

1000 °C because of our furnace limitation), the oxygen potential of Al₂O₃ is lower than the oxygen potential of the H₂/H₂O mixing gas. So, Al is oxidized to Al₂O₃ by H₂O. While, the oxygen potential of Cr, Fe, and Ni oxide is higher than the H₂/H₂O mixing gas, each metal oxide is resolved and oxygen is discharged in order to keep equilibrium. It is almost exactly consistent with the data of Ellingham's diagram.

B. Al₂O₃ film formation on as-welded bead

Figure 7 shows the XPS depth profile of a welded bead by flowing through the various backshield gases. The horizontal axis shows film thickness and the vertical axis shows atomic concentration. When only using the 5% H₂/Ar gas for the backshield gas, it can be reformed as the Al₂O₃ passivation film on the welded bead. This is because the H₂ gas and background H₂O concentration level (0.1 ppb) included in the backshield gas when the applied residual temperature of the welding process is adjusted in condition to oxidize only the aluminum, according to the Ellingham diagram. Then, Cr, Ni, Mo, and Fe become reduced in this condition. In the case of only the Ar gas or trace amounts of oxygen in the Ar for use as the back shield gas, it was not possible to reform

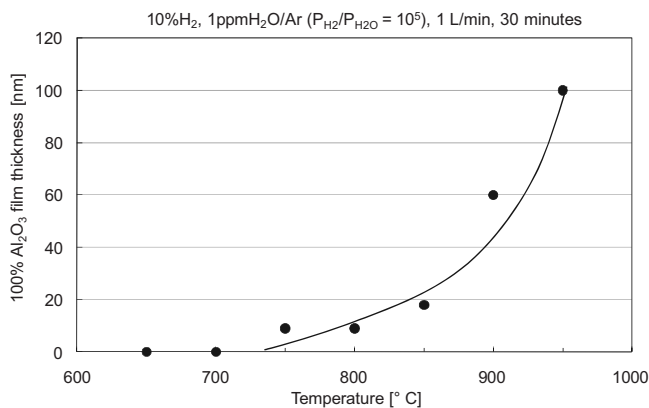


FIG. 6. Relationship between 100% Al₂O₃ film thickness and the treatment temperature for 30 min of oxidation in the ambient of $P_{H_2}/P_{H_2O}=10^5$.

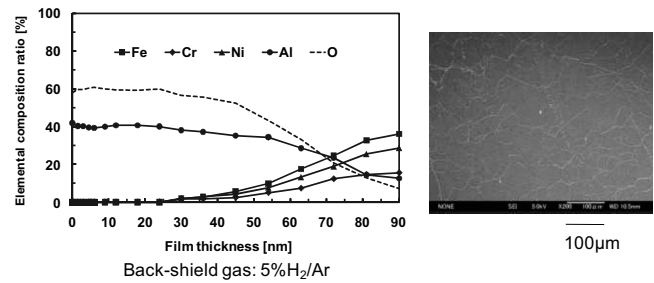


FIG. 7. XPS depth profile and SEM photograph of welded bead by flowing through 5% H₂/Ar backshield gases.

the Al₂O₃ passivation film free of other elements on the welded bead in our experiments. From SEM observation, the welded bead when using the 5% H₂/Ar backshield gas looks like a smooth surface. The Al₂O₃ passivation film included on the welded bead was fabricated by introducing this as-welded method. It can build up all over the gas tubing system, including the valve, welded fitting, and exhaust duct covered by the Al₂O₃ passivation film's inner surface.

C. Plasma resistance

We have evaluated plasma resistance for various gases by means of SEM observation and XPS depth profile of halogen elements. Figure 8 shows the relationship between the reaction quantity of the fluorine element in depth profile and ion-bombardment energy with NF₃ plasma for 1 h. The vertical axis shows the reaction quantity of the fluorine element in the depth profile. The horizontal axis shows the ion-bombardment energy. Figure 9 shows the SEM images before and after exposure to the NF₃ plasma with ion-bombardment energy of 80 eV for 1 h. In the case of the conventional SUS316L-EP surface and the Cr₂O₃ passivated stainless-steel surface, the amount of elemental fluorine at depth increases with the increase in the ion-bombardment energy. From the SEM observation, the SUS316L-EP and Cr₂O₃ passivated stainless-steel surfaces were damaged deeply. While in the case of the Al₂O₃ passivated stainless-

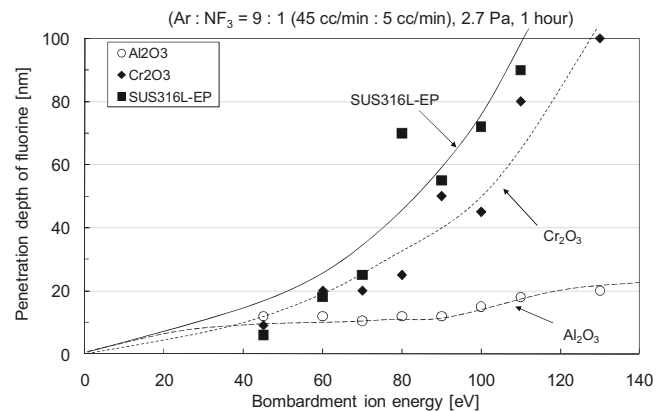


FIG. 8. Penetration depth of fluorine is plotted as a function of bombarding ion energy of NF₃ RF excited plasma where SUS316L-EP surface, Cr₂O₃ passivated surface, and Al₂O₃ passivated surface are exposure to NF₃ plasma for 1 h.

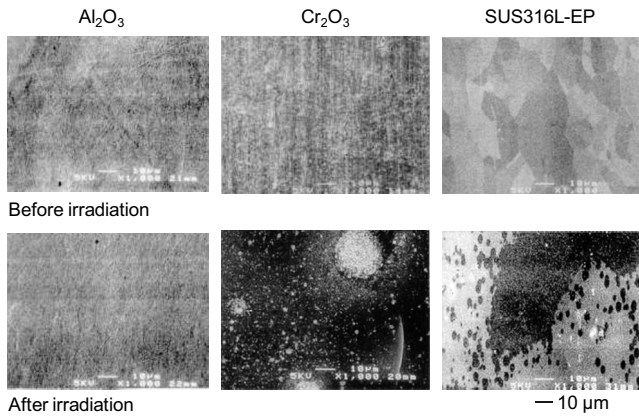


FIG. 9. SEM images of Al₂O₃, Cr₂O₃, and SUS316L-EP stainless-steel surfaces before and after the exposure to the NF₃ plasma (10% NF₃/Ar, 50 cc/min, 2.7 Pa, bombardment ion energy=80 eV, 20 °C, 1 h).

steel surface, the reaction quantity of the fluorine element in the depth profile stopped at about 15 nm, in spite of the ion-bombardment energy increasing. Moreover, the surface condition is also very good after plasma irradiation. Figures 10–12 show the XPS depth profile before and after the exposure to the NF₃ plasma with ion bombardment energy of 80 eV for 1 h. In the case of the SUS316L-EP surface and the Cr₂O₃ passivated stainless-steel surface, chromium fluoride, iron fluoride, and nickel fluoride are generated at the top of the surface. In the case of some fluoride materials, it may be etched off by a H radical or vaporized. While, in the case of Al₂O₃ passivated stainless-steel, 15 nm of Al₂O₃ film from the top of the surface is replaced by a F atom lower than 80 eV of ion-bombardment energy for NF₃ plasma. But AlF₃ film generated by NF₃ plasma irradiation is thermodynamically very stable, as well as Al₂O₃ (Table II). Figure 13 shows the relationship between the temperature of the specimen and the reaction quantity of fluorine. It is shown that the dependence on temperature of fluorine reaction is very small at the Al₂O₃ passivated stainless-steel surface. It is proven that the Al₂O₃ passivated stainless-steel surface has strong resistance for fluorinated-gas plasma. Al₂O₃ passivated stainless-steel shows an excellent resistance performance in the fluorinated-gas plasma environment.

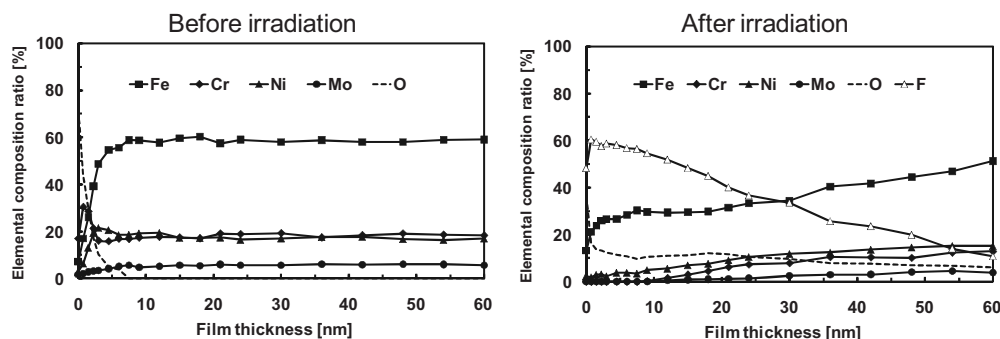


FIG. 10. XPS depth profile of SUS316L-EP stainless-steel surface before and after the exposure to the NF₃ plasma with bombardment ion energy of 80 eV for 1 h.

Figure 14 shows the relationship between the reaction quantity of the chlorine element in depth profile and ion-bombardment energy with Cl₂ plasma for 1 h. The vertical axis shows the reaction quantity of the chlorine element in depth profile. The horizontal axis shows ion-bombardment energy. We have experimented in the range of ion-bombardment energy below 130 eV. Figure 15 shows the SEM images before and after exposure to the Cl₂ plasma with ion-bombardment energy of 80 eV for 1 h. In the case of the conventional SUS316L-EP surface and Cr₂O₃ passivated stainless-steel surface, the reaction quantity of chlorine in the depth profile increases with the increase in the ion-bombardment energy. From the SEM observation, the SUS316L-EP and the Cr₂O₃ passivated stainless-steel surface were damaged deeply. While in the range of ion-bombardment energy lower than 80 eV, the Al₂O₃ passivated stainless-steel surface does not permit reaction with chlorine. By observing the SEM image in the range of ion-bombardment energy lower than 80 eV, it is found that the Al₂O₃ passivated stainless-steel surface has no damage from the Cl radical. This result confirms that corrosion was not observed on the stable Al₂O₃ surface after it was exposed to reactive Cl radicals and ions. Figure 16 shows the relationship between the temperature of the surface and the reaction quantity of the chlorine element in the depth profile. The Al₂O₃ passivated stainless-steel surface does not permit reaction with chlorine at temperatures below 150 °C.

Figure 17 shows the relationship between oxide-film-thickness variation and ion-bombardment energy with O₂ plasma for 1 h. The vertical axis shows the variation in oxide-film-thickness after O₂ plasma irradiation. The horizontal axis shows ion-bombardment energy. We have experimented in the range of ion-bombardment energy below 130 eV. In the case of the conventional SUS316L-EP surface, the oxide-film-thickness increases with the increase in the ion-bombardment energy. This figure shows that the oxygen radical got into the SUS316L-EP surface. In the case of Cr₂O₃ passivated stainless-steel having 20 nm film thickness, oxide-film-thickness decreases with the increase in the ion-bombardment energy over 80 eV. These data show that Cr₂O₃ is oxidized to CrO₃ by the oxygen radical and that CrO₃ disappeared because of its high vapor pressure. In con-

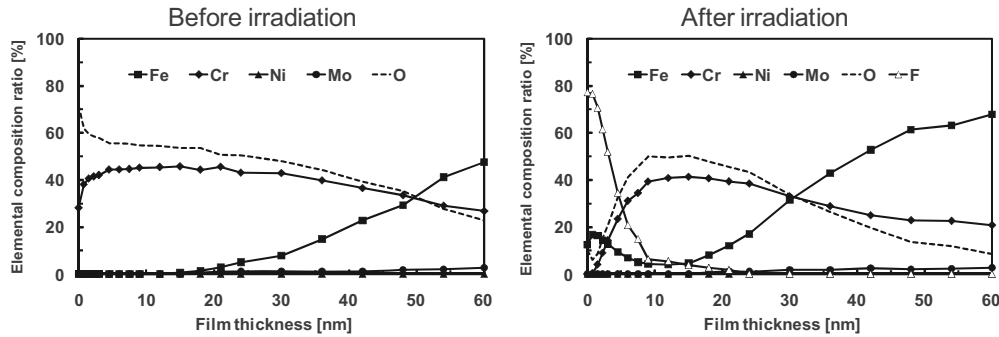


FIG. 11. XPS depth profile of Cr₂O₃ passivated stainless-steel surface before and after the exposure to the NF₃ plasma with bombardment ion energy of 80 eV for 1 h.

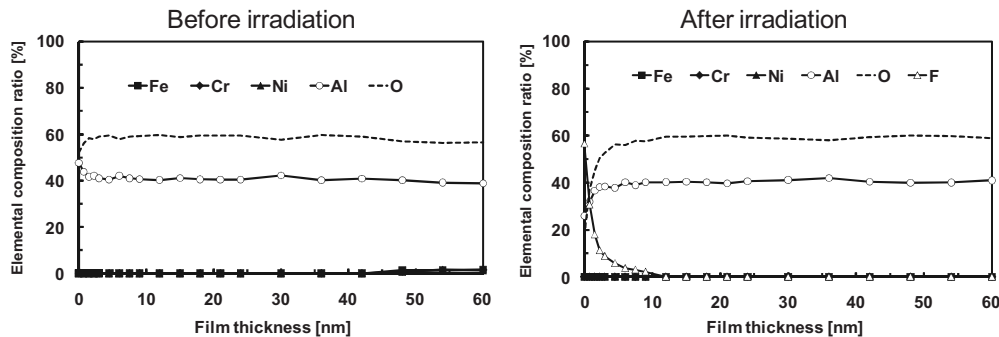


FIG. 12. XPS depth profile of Al₂O₃ passivated stainless-steel surface before and after the exposure to the NF₃ plasma with bombardment ion energy of 80 eV for 1 h.

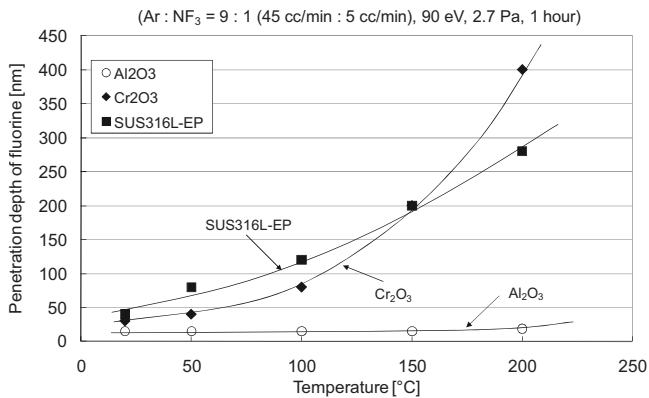


FIG. 13. Penetration depth of fluorine vs sample temperatures where the sample surfaces are exposed to the NF₃ plasma for 1 h with bombarding ion energy of 90 eV.

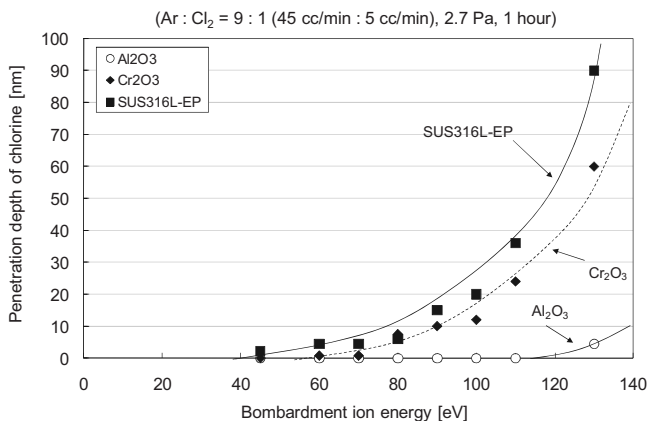


FIG. 14. Penetration depth of chlorine vs bombardment ion energy of Cl₂ RF excited plasma where the samples such as Al₂O₃, Cr₂O₃, and SUS316L-EP stainless-steel are exposed to the Cl₂ plasma for 1 h.

trast, in the range of plasma potential lower than 130 eV, the Al₂O₃ passivated surface did not permit reaction of the oxygen radical. The change in oxide-film-thickness was not observed completely at the Al₂O₃ passivated stainless-steel surface.

Moreover, in our study, Al₂O₃ passivation film does not completely receive the damage or is not etched off by hydrogen ion-bombardment energy lower than 130 eV.

D. Catalytic activity

It is well known that metal surfaces such as Ni and Pt have a catalytic activity. In the case of semiconductor manufacturing, this process causes unnecessary process-gas decomposition on the metal surfaces such as the gas-supply system, process chamber, and gas-exhaust system. In the case of the process chamber or the gas-supply system, it induces process fluctuation and reduction in the manufacturing yield. Or, in the case of the exhaust system, unexpected thermal decomposition in a pumping system or in the inside of an exhaust duct causes fluctuation of pumping speed. We must remove these fluctuation factors to create a highly productive manufacturing system. So, we examined the chemical inactivity of Al₂O₃ passivation film on stainless-steel, compared with other materials.

Figure 18(a) shows the thermal decomposition property for a 100 ppm concentration of SiH₄, B₂H₆, PH₃, AsH₃, and ClF₃ balanced Ar gas on the Al₂O₃ passivated stainless-steel surface. The vertical axis shows the concentration of specialty gases in Ar gas at the reactor-tube outlet. The horizontal axis shows the temperature of the Al₂O₃ passivated tube.

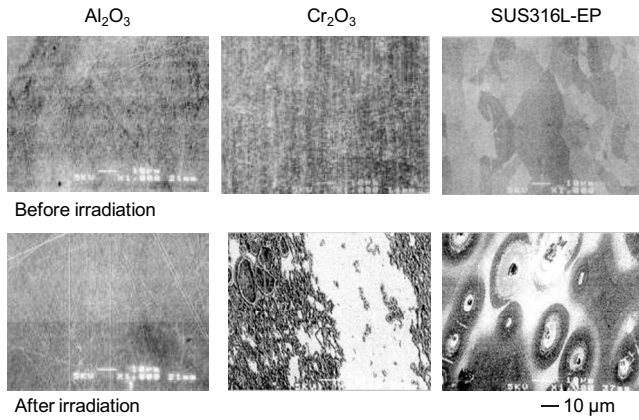


FIG. 15. SEM images of Al₂O₃, Cr₂O₃, and SUS316L-EP stainless-steel surfaces before and after the exposure to the Cl₂ plasma (10% Cl₂/Ar 50 cc/min, 2.7 Pa, bombardment ion energy=80 eV, 20 °C, 1 h).

B₂H₆ gas was decomposed at the lowest temperature of 150 °C, compared with other gases. And, next, ClF₃, AsH₃, PH₃, and SiH₄, gases began to be decomposed at about 160, 260, 320, and 380 °C, respectively. In contrast, on the SUS316L-EP surface, which is one of the most popular materials in semiconductor manufacturing equipment, AsH₃, ClF₃, B₂H₆, PH₃, and SiH₄ began to be decomposed at about 25, 50, 70, 120, and 320 °C, respectively, lower than the Al₂O₃ passivated surface [Fig. 18(b)]. Moreover, on the Ni surface, these gases decomposed at even lower temperatures than the Al₂O₃ passivated stainless-steel surface and the SUS316L-EP surface [Fig. 18(c)]. Some specialty gases began to decompose even at near the room temperature on the Ni surface. The Ni surface has a strong catalytic effect for thermal decomposition of various hydride gases. These results indicate that the Al₂O₃ passivated surface never assists thermal decomposition of these gases at lower than 150 °C. Briefly, the *d*-electrons of the metal afford chemical bonding opportunities that are unavailable on the metal oxide surfaces.¹⁶ So, it is hard for the decomposition of hydride gases to occur on the insulated film surface such as Al₂O₃ passivated surface.

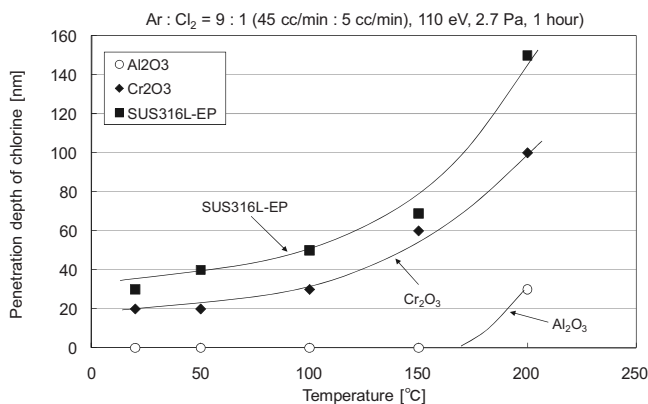


FIG. 16. Penetration depth of chlorine vs sample temperatures where the sample surfaces are exposed to the Cl₂ plasma for 1 h with bombarding ion energy of 110 eV.

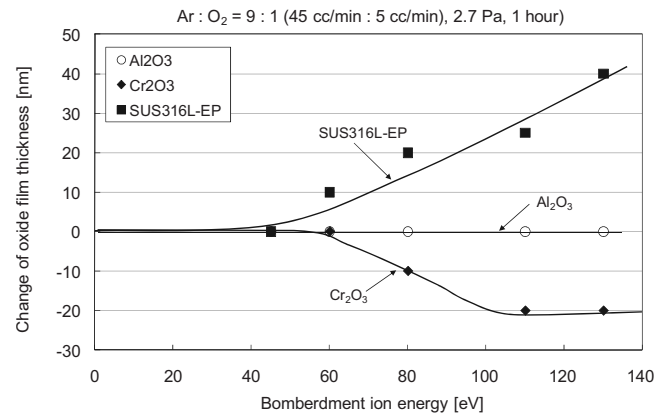


FIG. 17. Change in oxide film thickness vs bombarding ion energy O₂ plasma where the sample surfaces are exposed to the O₂ plasma for 1 h.

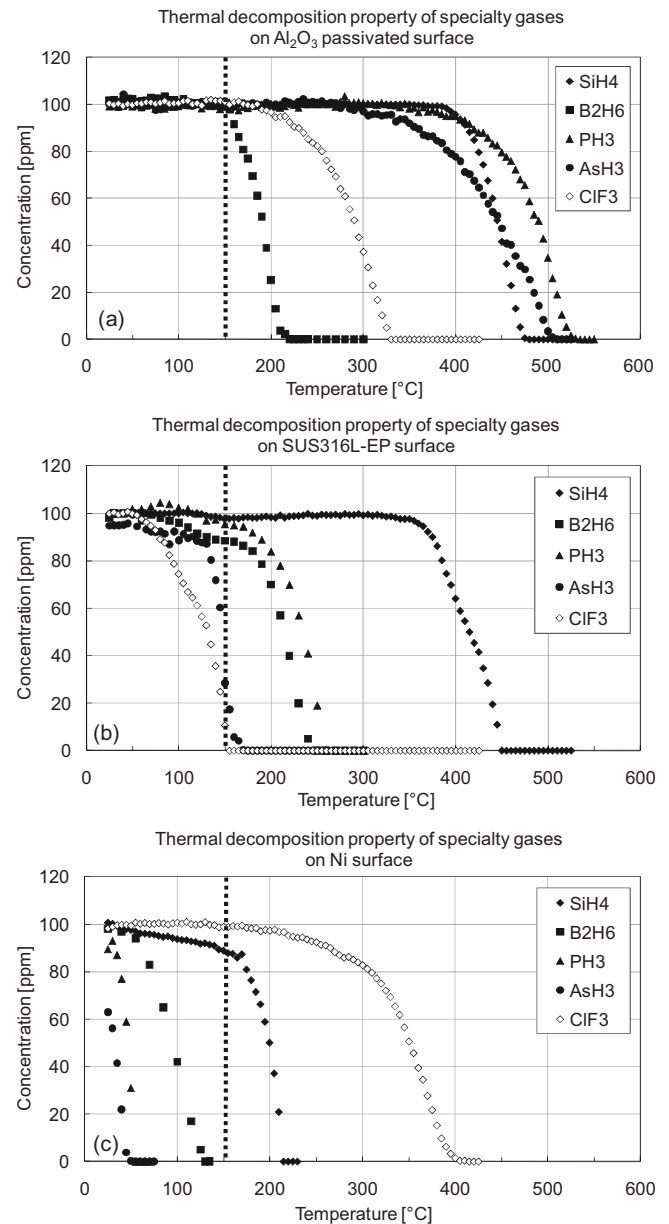


FIG. 18. Concentration of various specialty gases such as SiH₄, B₂H₆, PH₃, AsH₃, and ClF₃ just after passing through tube of 1/4 inch of 1 m length whose inner surface is (a) Al₂O₃ passivated, (b) SUS316L-EP, and (c) Ni vs tube temperature, where the initial specialty gas concentration is maintained at 100 ppm in Ar gas.

The mechanism of ClF₃ gas decomposition is different from the hydride-gas case on a metal surface. ClF₃ gas directly reacts with various metal surfaces at predetermined temperature. It is found that the metal fluoride was formed after the ClF₃ decomposition specimen by the reaction with fluorine released from ClF₃ gas dissociation. Chlorine was not detected at all by XPS analysis. So, we considered that the decomposition of ClF₃ gas is limited by the ease of the fluorine and metal-surface reaction. Thus, the concentration of ClF₃ decreases on metal surface. If the temperature of decomposition becomes higher, it means that such a surface is stable for ClF₃ gas. It is very interesting that the Ni, which showed highly catalytic activity to the hydride gases, is the most stable for the ClF₃ gas. In the case of Al₂O₃ passivation film, ClF₃ does not decrease until 160 °C. It is very stable compared with the general SUS316L-EP surface. Moreover, AlF₃ generated by the reaction with ClF₃ is thermodynamically very stable, as is Al₂O₃.

IV. CONCLUSION

We have established the selective-oxidation technology of the newly developed austenitic stainless steel containing 3 wt % aluminum, where the excellent Al₂O₃ passivation films having very high anticorrosion capability have been formed in the ambient atmosphere of $P_{H_2}/P_{H_2O} \cong 1 \times 10^4$ at temperatures higher than 750 °C. Newly developed Al₂O₃ passivation films have been confirmed to exhibit excellent plasma resistance for various gas-plasma environments such as fluorine gas, chlorine gas, hydrogen gas, oxygen gas, etc. at temperatures less than 150 °C for bombarding ion energies less than 80 eV. Moreover, the Al₂O₃ passivation films have been confirmed not to exhibit catalytic behavior for the decomposition of various specialty gases at temperatures less than 150 °C, where various specialty gases, including B₂H₆, do not decompose at temperatures up to 150 °C. In order to establish very-high-productivity manufacturing of semiconductor devices, large-size flat-panel displays, and new silicon

thin-film solar cells, very new processes, such as different thin-film continuous deposition or etching only by changing process gases in the same process chamber, must be developed. This must occur where there exist essential requirements of the excellent Al₂O₃ passivation films having very high anticorrosion resistance and no catalytic behavior, such as decomposing various specialty gases at very low temperatures.

- ¹T. Ohmi, M. Hirayama, and A. Teramoto, *J. Phys. D* **39**, R1 (2006).
- ²Y. Saito, K. Sekine, M. Hirayama, and T. Ohmi, *Jpn. J. Appl. Phys.* **38**, 2329 (1999).
- ³K. Sekine, Y. Saito, M. Hirayama, and T. Ohmi, *J. Vac. Sci. Technol. A* **17**, 3129 (1999).
- ⁴K. Sekine, Y. Saito, M. Hirayama, and T. Ohmi, *1999 Symposium on VLSI Technology Digest of Technical Papers*, Kyoto (Japan Society of Applied Physics, Tokyo, 1999), p. 115.
- ⁵M. Hirayama, K. Sekine, Y. Saito, and T. Ohmi, *Technical Digest, International Electron Devices Meeting*, Washington, D.C. (IEEE, New York, 1999), p. 249.
- ⁶Y. Saito, K. Sekine, N. Ueda, M. Hirayama, S. Sugawa, and T. Ohmi, *2000 Symposium on VLSI Technology Digest of Technical Papers*, Honolulu (IEEE, New York, 2000), p. 176.
- ⁷T. Goto, K. Ikenaga, A. Teramoto, M. Hirayama, S. Sugawa, and T. Ohmi, *J. Vac. Sci. Technol. A* **26**, 8 (2008).
- ⁸T. Ohmi, M. Hirayama, T. Goto, A. Inokuchi, M. Kitano, and M. Tahara, *WPI-AIMR (Tohoku University), News* **8**, 93 (2009).
- ⁹Y. Kawase, M. Kitano, F. Mizutani, M. Saeki, Y. Shirai, and T. Ohmi, *J. Electrochem. Soc.* **154**, C530 (2007).
- ¹⁰Y. Shirai, M. Narazaki, and T. Ohmi, *IEICE Trans. Electron.* **79-C**, 385 (1996).
- ¹¹T. Ohmi, A. Ohki, M. Nakamura, K. Kawada, T. Watanabe, Y. Nakagawa, S. Miyoshi, S. Takahashi, and M. S. K. Chen, *J. Electrochem. Soc.* **140**, 1691 (1993).
- ¹²M. Yoshida, A. Seki, Y. Shirai, and T. Ohmi, *J. Vac. Sci. Technol. A* **17**, 1059 (1999).
- ¹³T. Ohmi, S. Miyoshi, Y. Shirai, T. Kojima, and Y. Mizuguchi, *J. Electrochem. Soc.* **142**, 2362 (1995).
- ¹⁴F. D. Richardson and J. H. E. Jeffes, *J. Iron Steel Inst., London* **160**, 261 (1948).
- ¹⁵H. J. T. Ellingham, *J. Soc. Chem. Ind. Trans.* **63**, 125 (1944).
- ¹⁶J. Greeley, J. K. Norskov, and M. Mavrikakis, *Annu. Rev. Phys. Chem.* **53**, 319 (2002).